JOURNAL OF GEOPHYSICAL RESEARCH: OCEANS, VOL. 118, 5322–5332, doi:10.1002/jgrc.20379, 2013

Large-scale alignment of oceanic nitrate and density

Melissa M. Omand[1] and Amala Mahadevan[1]

Received 1 May 2013; revised 1 August 2013; accepted 26 August 2013; published 15 October 2013.

[1] By analyzing global data, we find that over large scales, surfaces of constant nitrate are often better aligned with isopycnals than with isobars, particularly below the euphotic zone. This is unexplained by the movement of isopycnal surfaces in response to eddies and internal waves, and is perhaps surprising given that the biological processes that alter nitrate distributions are largely depth dependent. We provide a theoretical framework for understanding the orientation of isonitrate surfaces in relation to isopycnals. In our model, the nitrate distribution results from the balance between depth-dependent biological processes (nitrate uptake and remineralization), and the along-isopycnal homogenization of properties by eddy fluxes (parameterized by eddy diffusivity). Where the along-isopycnal eddy diffusivity is relatively large, nitrate surfaces are better aligned with isopycnals than isobars. We test our theory by estimating the strength of the eddy diffusivity and biological export production from global satellite data sets and comparing their contributions. Indeed, we find that below the euphotic zone, the mean isonitrate surfaces are oriented along isopycnals where the isopycnal eddy diffusivity is large, and deviate where the biological export of organic matter is relatively strong. Comparison of nitrate data from profiling floats in different regions corroborates the hypothesis by showing variations in the nitrate-density relationship from one part of the ocean to another.

Citation: Omand, M. M., and A. Mahadevan (2013), Large-scale alignment of oceanic nitrate and density, *J. Geophys. Res. Oceans*, *118*, 5322–5332, doi:10.1002/jgrc.20379.

1. Introduction

[2] Inorganic nitrate is one of the important macronutrients for oceanic phytoplankton and provides the nitrogen that forms about 16% of the stoichiometric biomass of phytoplankton cells. Dissolved inorganic nitrate (henceforth referred to as nitrate) is typically abundant in the deep ocean, where it is restored through the remineralization of organic matter, and depleted near the surface, where it is consumed by phytoplankton production and thereby converted to particulate organic matter. Since dissolved carbon is abundant in the oceans, phytoplankton production is largely limited by the availability of light and nutrients, such as nitrate. Vast regions of the surface sunlit oceans are oligotrophic or macronutrient-depleted, and phytoplankton production is dependent on the supply of nutrients into the euphotic zone from the subsurface, from ocean margins, fixation of dissolved gases or atmospheric deposition. Rotation and stratification restrict the vertical movement of water and extremely weak rates of mixing across isopycnal surfaces inhibit the vertical exchange of nitrate across the pycnocline, which results in a vertical gradient of nitrate in what is often referred to as the twilight zone, the region that extends a few hundred meters downward from the base of the euphotic zone.

[3] The vertical distribution of nitrate on large scales is of particular interest in understanding the oceanic biological pump. Locally, the vertical flux of nitrate into the euphotic zone depends not only on the underlying dynamics but also on the vertical gradient of nitrate and depth of nitracline beneath the summertime surface mixed layer. An increasing abundance of nitrate measurements has given us insight into the large-scale, global distribution and variability of nitrate. Ship-board measurements have generated global databases for nitrate [*Kamykowski and Zentara*, 1985; *Levitus et al*., 1993], and more recently, nitrate profiling floats have enabled sampling spatiotemporal variability on space-time scales of kilometers and days [*Johnson et al*., 2010, 2013]. These studies, along with those with a more regional focus, such as *Lucas et al*. [2011], have revealed a relationship between oceanic density (or temperature) and nitrate distribution in the vertical. This relationship forms the basis of for estimating surface nitrate, and consequently new production, from remotely sensed temperature data [*Goes et al*., 2000; *Switzer et al*., 2003] in regions where nitrate is a limiting nutrient for phytoplankton. It has also been used for the initialization of nitrate in ocean models.

[4] Recent studies have analyzed the variability of nitrate on isobars and isopycnals. *While and Haines* [2010] calculate the variance of the measured nitrate from profiles that constitute the World Ocean Atlas within $2^\circ \times 2^\circ$ bins.

[1]Woods Hole Oceanographic Institution, Woods Hole, Massachusetts, USA.

Corresponding author: M. M. Omand, Woods Hole Oceanographic Institution MS 29, Woods Hole, MA 02543-1050, USA. (momand@whoi.edu)

©2013. American Geophysical Union. All Rights Reserved.
2169-9275/13/10.1002/jgrc.20379

They find the variance is larger at constant depth than on constant density (σ_t) surfaces. They ascribe the higher variance at fixed depth to ocean dynamics including internal waves and eddies, which cause isopycnal surfaces to heave and sink, contributing variability among profiles taken at different positions and times. *Ascani et al*. [2013] analyze the nitrate measured from profiling floats in the upper subtropical North Pacific Ocean and find the variance of nitrate on isobars to be larger than on isopycnals. This is largely due to the transient movement of isopycnal surfaces by eddies, which they identify from the anticorrelation in isopycnal displacement and sea surface height.

[5] When we analyze the locally binned and smoothed nitrate data on global scales, we find that nitrate in the twilight zone (roughly between 200 m and 600 m) also shows greater variability on isobars than on isopycnals (Figure 1). The relationship of nitrate to density persists over scales much larger than eddies and in most regions (though not everywhere) surfaces of constant nitrate (isonitrate surfaces) are more aligned with isopycnals than with depth. This cannot be attributed to short timescale eddy and internal wave dynamics. It poses a paradox because processes that alter nitrate are depth dependent. Phytoplankton production relies on light, which varies exponentially with depth, and the remineralization of organic matter falls off exponentially (or with a power law) beneath the euphotic layer. Hence, one might expect nutrient to be more strongly related to depth than density, based on the depth-dependence of its sources and sinks. Instead, we find a persistence in the co-orientation of nitrate with density surfaces, indicating that the redistribution of nitrate is not just a one-dimensional process.

[6] One explanation is that in the case where the isopycnals are sloping, the orientation of isonitrate surfaces relative to isopycnals depends on the strength of the depth-dependent biological processes that consume and release nitrate, relative to the strength of the eddying field, which tends to homogenize tracers along isopycnal surfaces by stirring gradients. If the biological pump is strong compared to the tendency of the along-isopycnal eddy-diffusivity to homogenize along isopycnals, one can expect the nitrate surfaces to be oriented perpendicular to gravity. If the effect of eddy-driven stirring is strong compared to the biological pump, we would expect the nitrate to be oriented along isopycnals.

[7] In what follows, we begin by analyzing the nitrate data from the World Ocean Atlas to compare the slope of isopycnal and isonitrate surfaces over the globe. We then use a model to demonstrate mechanistically how by varying (weakening) the strength of the biological pump compared to along-isopycnal eddy diffusivity, one can change the orientation of isonitrate surfaces from flat (horizontal) to along-isopycnal. We show that the variability of nitrate along density and depth surfaces varies amongst different regions of the world's oceans, but can be explained on the basis of the strength of the biological pump compared to the effect of along-isopycnal mixing.

2. Mean Global Distributions of Nitrate and Density

2.1. Data

[8] We use the $5^\circ \times 5^\circ$ ($n = 2448$ gridded bins), annually averaged nitrate (NO_3) and potential density σ_t, from the World Ocean Atlas (WOA09) [*Garcia et al*., 2010] available through the National Oceanographic Data Center (http://www.nodc.noaa.gov/OC5/SELECT/dbsearch/dbsearch.html). The dataset compiles roughly 50 years of ship-based profiles of nitrate into a monthly climatology. The vertical bin size varies from 10 m near the surface to 400 m below 2000 m depth. Due to the unequal geographic sampling effort and samples taken at different times of year, there are abrupt variations evident among adjacent grid cells in some places. To eliminate such grid-scale variability (noise) in the data, we construct objective maps of NO_3 and σ_t at each vertical level, with a noise-to-signal criterion of 10%, and a zonal and meridional decorrelation scale of 20° and 10° respectively [*Bretherton et al*., 1976]. The smoothing helps to remove some spurious ridges and speckling in the maps, but does not alter the large-scale patterns in the NO_3 and σ_t.

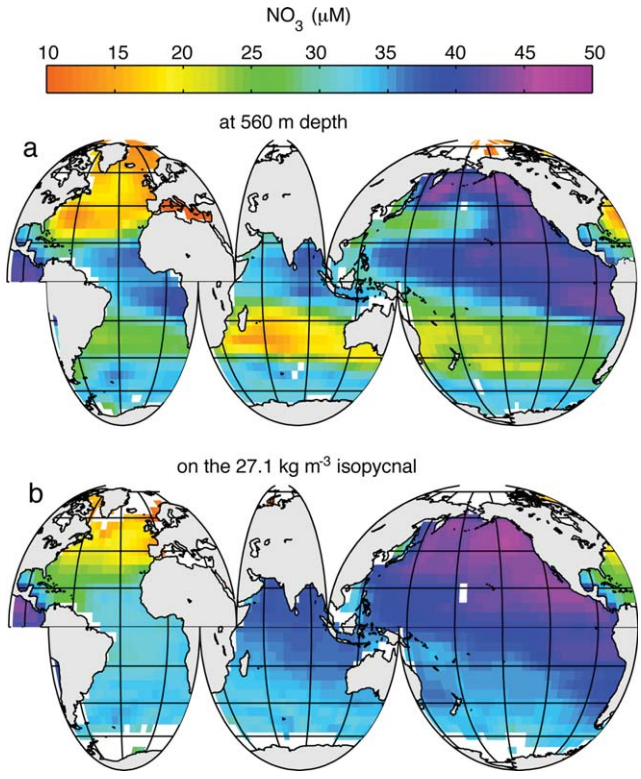

Figure 1. Climatological annual averages from the 5° WOA09 database; (a) NO_3 (μM) at 600 m and (b) NO_3 on the 27.5 kg m^{-3} isopycnal, the depth of which is centered at 560 m.

[9] Because our focus is on twilight zone distributions, we exclude NO_3 from within the euphotic zone, or maximum winter mixed layer depth, whichever penetrates deepest in the water column over the year. Solar irradiance is absorbed exponentially with depth over a length scale that is inversely related to the diffuse attenuation coefficient. The euphotic depth is defined as the depth where light is 1% of its surface value and estimated from the diffuse attenuation coefficient at 490 nm wavelength from the monthly Level 3 SeaWiFS product (K_{490}, http://oceancolor.gsfc.nasa.gov/) according to $z_{eu} = \log(0.01)/K_{490}$. We also obtain the monthly Level 3 mixed layer depth

climatology based on a criterion of 0.03 kg m^{-3} density variation from the surface (*de Boyer Montégut et al*. [2004] http://www.ifremer.fr/cerweb/deboyer/mld/home.php) and find the deepest monthly wintertime mixed layer depth. We interpolate these values onto the 5°×5° WOA09 grid and exclude any NO_3 shallower than these depths.

[10] For the analysis presented here, we select the 560 m WOA09 depth level; which is below the maximum global climatological euphotic depth (max. 196 m) and wintertime mixed layer (max. 526 m). At $z = -560$ m, and the levels bordering above ($z = -470$ m) and below ($z = -648$ m), there are roughly 100,000 WOA09 individual observations of NO_3 that are compiled into the climatology. At this depth, there is little seasonal change in NO_3 relative to the large scale patterns, and the annual climatology is appropriate for our analysis. At $z = -560$ m, the median potential density (σ_t) is 27.1 kg m^{-3}. We interpolate both NO_3 and σ_t onto a 1 m vertical grid, and obtain NO_3 on the $\sigma_t = 27.1$ kg m^{-3} isopycnal. The following analysis of isonitrate and isopycnal alignment is based on the horizontal gradients of NO_3 and σ_t at $z = -560$ m and vertical gradients between the bordering levels ($z = -648$ m and -470 m).

2.2. Large-Scale Variability of NO_3 on Isobars and Isopycnals

[11] We begin by examining and comparing the large-scale patterns in NO_3 at 560 m, and on the $\sigma_t = 27.1$ isopycnal surface. In general, the NO_3 concentration at 560 m depth is reduced in the subtropical gyres, and is elevated near the equator, Southern Ocean, and Eastern Pacific. The maximum NO_3 concentration is 11.3 μM in the Mediterranean Sea, and 45.6 μM in the North Pacific Ocean (Figure 1a). In many locations, there are relatively abrupt transitions in the NO_3 concentration, particularly at mid- and low-latitudes (<45°N).

[12] Nitrate on the 27.1 kg m^{-3} isopycnal is much smoother, with few abrupt changes in NO_3 (Figure 1b). The total range of NO_3 is similar, and the regional patchiness of NO_3 is greatly reduced compared to that on the 560 m isobar. Particularly striking, are the apparent provinces of relatively homogeneous nitrate (<±2.5 μM variation) in the Southern hemisphere, the North Atlantic and the North Pacific. By performing this analysis on the global climatology of NO_3 we demonstrate that the time-averaged large-scale subeuphotic distribution of NO_3 is more variable on isobars, as compared to isopycnals. This suggests that thermocline ventilation and along-isopycnal eddy diffusivity may be dominant processes that homogenize nitrate on isopycnals within the regions identified above.

2.3. Slope and Orientation of Isopycnals and Isonitrate Surfaces

[13] In order to compare the alignment between density (σ_t) and nitrate (NO_3), we evaluate the slope and orientation angle of the isosurfaces centered at $z = -560$ m (the depth examined in the previous section). We estimate the slope from the objectively mapped annual climatology on a 5°×5° grid. We use centered finite differences to compute the spatial gradients of density (σ_x, σ_y, σ_z) in the x, y and z directions, where the magnitude of the total horizontal gradient (subscript H) is $\sigma_H = (\sigma_x^2 + \sigma_y^2)^{1/2}$. The same procedure is applied to the nitrate data to obtain the NO_3 gradients.

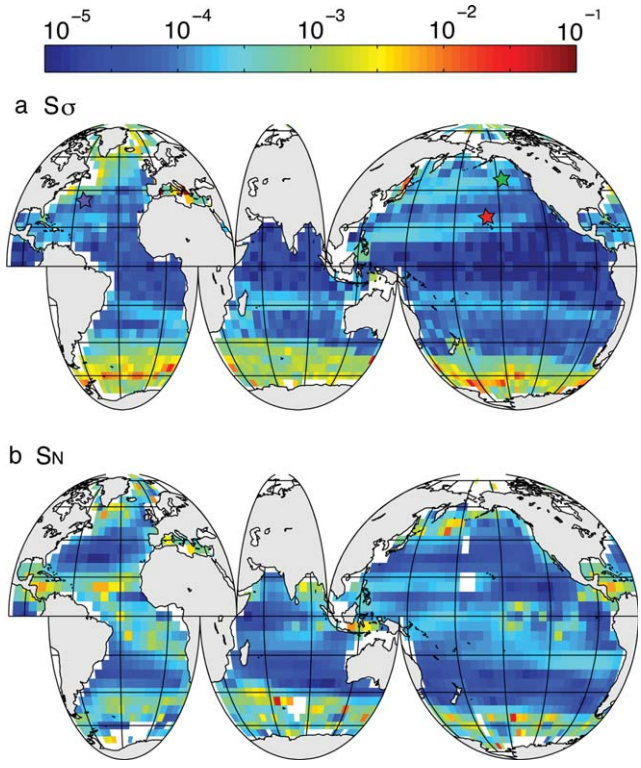

Figure 2. Large-scale slope of the (a) isopycnal (S_σ) and (b) iso-nitrate surfaces (S_N) at 560 m depth from the smoothed 5°×5° WOA09 climatology. The stars in (a) indicate the location of the APEX floats near Bermuda (blue), Hawaii (red), and Station Papa (green).

[14] The isopycnal and isonitrate slopes, S_σ and S_N, respectively, are computed from the ratio of the horizontal (subscript H) and vertical (subscript z) gradients of σ_t, and similarly NO_3 as

$$S_\sigma = \frac{\sigma_H}{\sigma_z}, \quad S_N = \frac{N_H}{N_z}. \tag{1}$$

[15] The isopycnal surfaces vary from being nearly horizontal ($S_\sigma < 10^{-5}$) near the equator to much steeper (S_σ ranges from 10^{-3} to 10^{-2}) at higher latitude (Figure 2a). The isonitrate surfaces similarly steepen at high latitudes (S_N ranges from 10^{-4} to 10^{-3}) and are nearly flat in the subtropical gyres (Figure 2b). Additionally, we see steeper isonitrate surfaces (higher S_N) near coastlines (e.g. west coast of North America) and in the Pacific and Atlantic equatorial regions. Both S_σ and S_N are roughly lognormally distributed. The isopycnal and isonitrate slopes are large only in a few places and the majority of the values lie below 10^{-3}, which corresponds to a vertical change of 100 m over 100 km or less.

[16] The orientation of the isopycnal (θ_σ) with respect to the eastward pointing vector (see Figure 3a) is calculated as

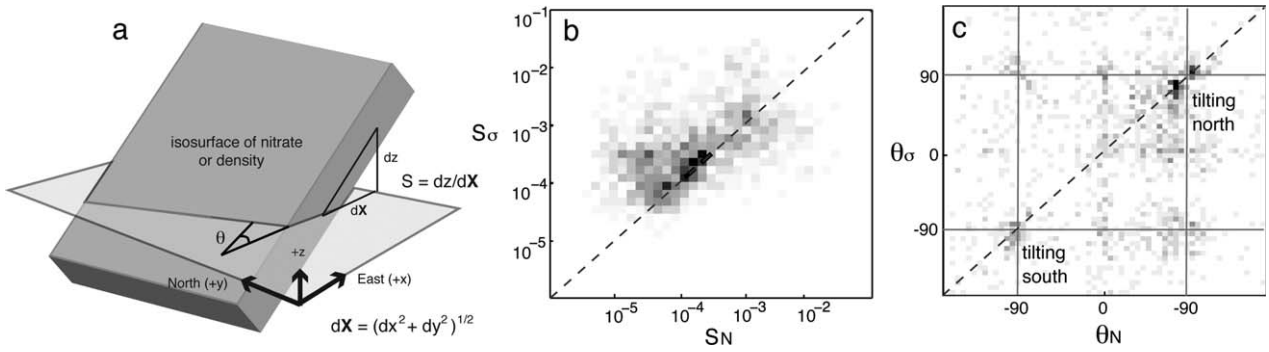

Figure 3. Schematic defining the slope (S) and orientation angle (θ) for the isosurfaces of NO_3 and σ_t. Histograms of the (a) isopycnal slope (S_σ) versus NO_3 isosurface slope (S_N) and (b) orientation angle for isopycnals (θ_σ) versus NO_3 (θ_N). Here, 90° indicates isosurfaces that are tilted up towards the north, and −90° indicates an upwards tilt toward the south. Both are derived from the WOA09 climatology at −560 m. Shading shows the number of grid points that fall into each bin, ranging from 0 to 22 and 11 for S and θ, respectively. The dashed line indicates the 1:1 line for each.

$$\theta_\sigma = \begin{cases} \tan^{-1}\dfrac{\sigma_x}{\sigma_y} + \pi, & \text{for } \sigma_x + \sigma_y < 0 \\ \tan^{-1}\dfrac{\sigma_x}{\sigma_y} - \pi, & \text{for } \sigma_y < 0 \text{ and } \sigma_x < 0 \\ \text{else} & \\ \tan^{-1}\dfrac{\sigma_x}{\sigma_y} & \end{cases} \quad (2)$$

[17] The same approach is applied to NO_3 to find the isonitrate orientation (θ_N). Orientations $\theta_\sigma = 0$ or $\theta_N = 0$ indicate the isopycnal or isonitrate surface is tilted upward toward the east, $\theta = 90°$ indicates tilting up toward the north, and $\theta = -90°$ indicates tilting up toward the south, in each case, with the slope S_σ and S_N. The slopes (S_σ and S_N) are weakly correlated, with $r^2 = 0.18$ (where the total number of points $n = 1333$).

[18] Further structure in the relationships is revealed by plotting the 2D histograms of S_σ vs. S_N (Figure 3b) and θ_σ vs. θ_N (Figure 3c). Here, we see that much of the data for both S and θ fall along the 1:1 line (dashed lines, Figures 3b and 3c), indicating locations where the density and nitrate surfaces are aligned. The bins that contain the most points also show a strong correlation. We quantify this finding for S_σ versus S_N, by applying a nearest-neighbor approach, and select only those data that have at least 7 points that are within a 0.05 range (in log-space). As anticipated, the correlation is significantly improved, with $r^2 = 0.45$, corresponding to the dense points represented by the darker-colored ridge in the histogram (Figure 3b). Similarly, the r^2 for θ_σ versus θ_N becomes 0.45 when points that have less than 30 neighbors within 10° are excluded. The improved correlation is not strongly sensitive to the choice of the nearest-neighbor criterion. These limits were selected such that at least 20% of the data are retained. By filtering according to the density of nearest neighbors, we are effectively removing outliers that are rare in S_σ-S_N (or θ_σ-θ_N) space, thus excluding all but the highest precision points that most clearly demonstrate the alignment between nitrate and density surfaces.

3. Regional and Temporal Variability of NO_3 on Isobars and Isopycnals

[19] Having examined the correlation between the average slope and orientation of nitrate surfaces at large scales, we now compare the temporal NO_3 variance on isopycnals and isobars from different oceanic regions. We use profiles from three NO_3-equipped APEX floats cycling at 5 day intervals, located near Bermuda (6391bermuda), Hawaii (6401hawaii) and Station Papa (5143stnp) and analyze a 500 day period from September 2009 to February 2011 when all three floats provided data. We examine data from $z < -150$ m, below the deepest annual euphotic depth at Hawaii. The profiles are interpolated and binned into 85 vertical bins in z (bin size = 10 m) and σ_t (with a bin size adjusted to span the observed dynamic range in σ_t). The timeseries at each depth (density) level is then low-passed with a 30 d (Gaussian half-width) filter in order to remove internal waves and higher frequency dynamics that would displace NO_3 and σ_t simultaneously. We perform this filtering because we are interested in regional differences in the NO_3-σ_t relationship over (seasonal and longer) timescales that are larger than those associated with waves and transient eddies.

[20] A nitracline is evident at 6391bermuda between −500 and −850 m (Figure 4a), between −300 and −500 m at 6401hawaii (Figure 4b), and between −200 and −400 m at 5143stnp (Figure 4c), and is indicated by the black vertical arrows in each time series. At 6391bermuda, the water column is strongly stratified with low-nutrients and a deep nitracline. 6401hawaii samples waters with lower density and weaker stratification, with NO_3 being negligible at −200 m and increasing to roughly 40 μM at −1000m. 5143stnp had higher nitrate (~32 μM) at −200 m, and sampled stratified waters between −200 and −400 m, with little variation in σ_t or NO_3 at depth. In density space (Figures 4d–4f) the NO_3, in general, shows less temporal variability.

[21] The variance of NO_3 at each z and σ_t bin is computed over a 90 day sliding window across the 500 day record at each 10 m bin, yielding a depth-resolved time series

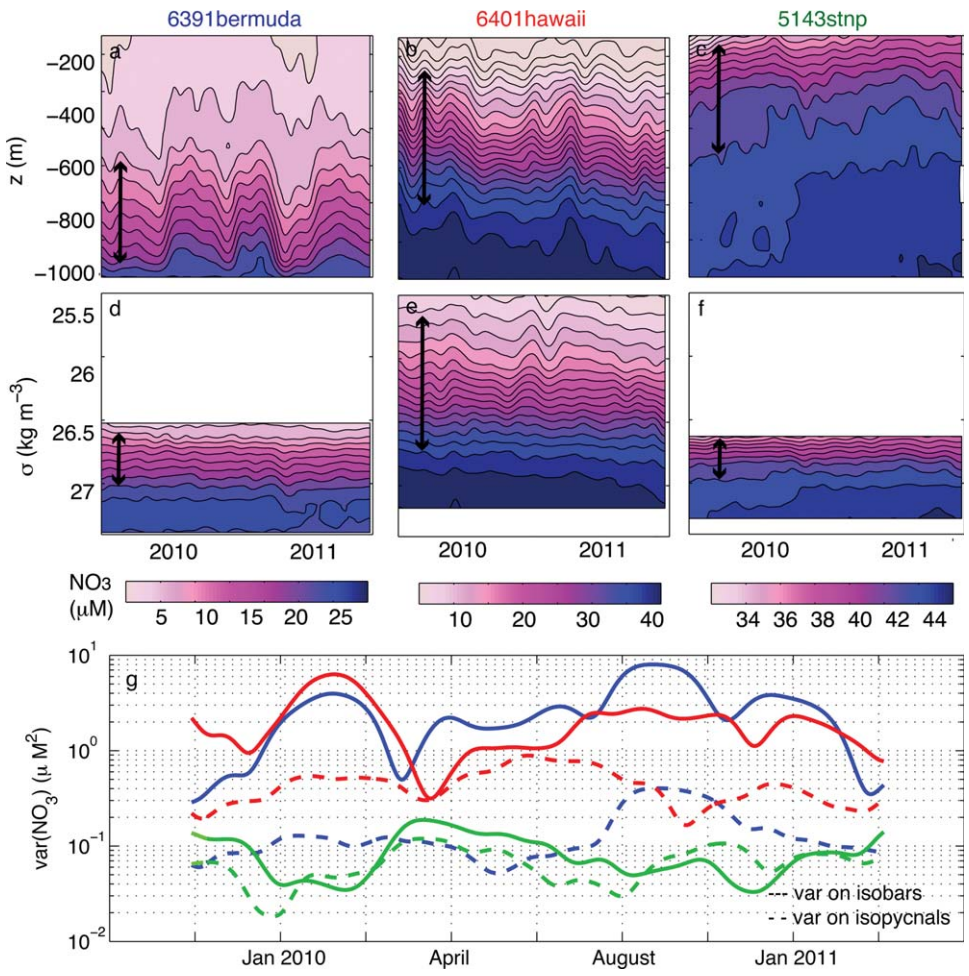

Figure 4. Contours of NO_3 in (a–c) depth and (e–g) density from three Nitrate-equipped APEX floats (a and d) 6391bermuda, (b and e) 6401hawaii, and (c and f) 5143stnp. The black arrows indicate the width of the nitracline region analyzed in each case. (g) Timeseries of the mean NO_3 variance averaged over the nitracline along isobars (solid lines) and isopycnals (dashed lines). The variance timeseries was computed within a sliding 90 day window for 6391bermuda (blue), 6401hawaii (red), and 5143stnp (green).

of temporal variance. The same method is applied to the NO_3 binned in σ_t-space. These variance time series are then vertically averaged over the nitracline indicated by the black arrows in Figures 4a–4f. For both 6391bermuda and 6401hawaii, the variance on isopycnals is up to 15 times smaller than the variance on isobars (compare the blue and red solid and dashed lines, Figure 4g). This difference is consistent throughout the year, suggesting that there are sustained processes that maintain the alignment of isonitrate and isopycnal surfaces in these subtropical regions. 5143stnp on the other hand, had a roughly equal balance of NO_3 variance between isobars and isopycnals, highlighting that these patterns are not consistent in all regions.

[22] In general, we find that the time-averaged NO_3 in the twilight zone is closely related to isopycnals. A similar analysis by *While and Haines* [2010] computed the spatial variance of NO_3, and found that the ratio between the NO_3 variance on isobars and isopycnals was larger than 1 for more than 79% of the global $5^\circ \times 5^\circ$ grid cells analyzed. *Ascani et al*. [2013] also used APEX profiling floats in the subtropical Pacific to explore the variance of NO_3 on isopycnals. They found that episodic shallow NO_3 anomalies are correlated with changes in the depth of the isopycnal surfaces. In this case, vertical isopycnal displacements associated with the balanced eddy field lead to enhanced localized NO_3 uptake, thus enhancing NO_3 gradients on isopycnals. We examine this relationship well below the euphotic zone at similar mid-latitudes (6401hawaii and 6391bermuda), and find that fluctuations in the temporal variance are relatively small compared with the time-averaged difference in the NO_3 variance on isobars or isopycnals.

4. What Sets the Slope of Isonitrate Surfaces?

[23] In the absence of lateral sources of NO_3, or local gradients in production, we anticipate that export and the biological resupply of NO_3 would orient isonitrate surfaces horizontally. In general, horizontal surface gradients in nitrate resulting from spatial variability in phytoplankton production and export, are much smaller than vertical gradients. In contrast, eddy-driven stirring and advection

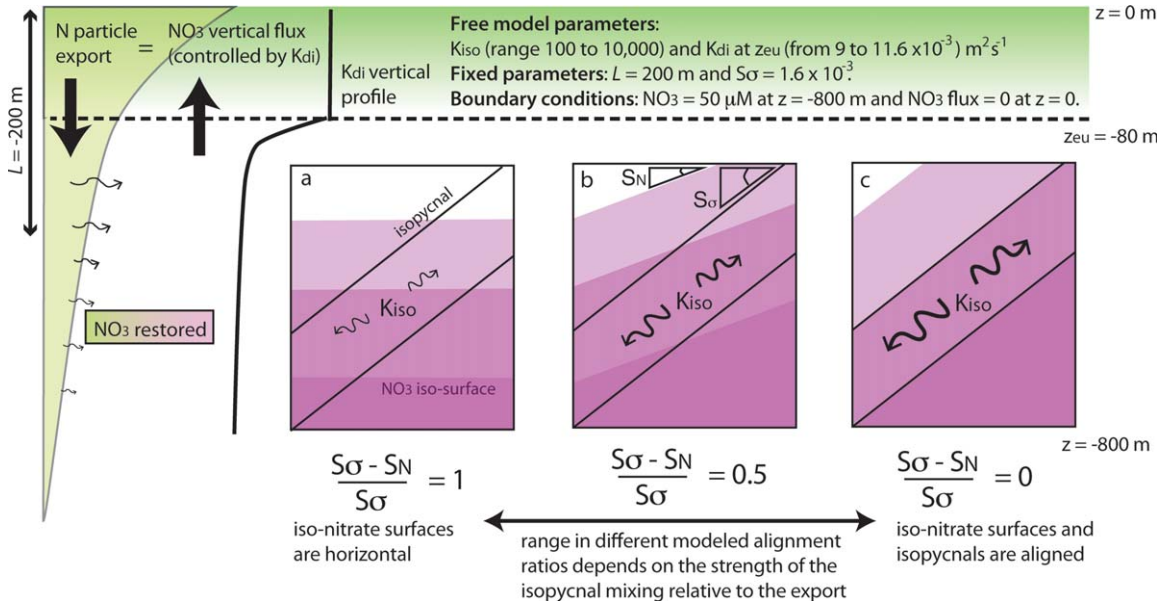

Figure 5. Schematic of the model set-up and three cartoon examples of steady state NO_3-isopycnal alignment. From left to right, the green exponential profile represents the shape of the modeled NO_3 restoration, with a remineralization scale L of 200 m. The bold arrows represent the balance between the total NO_3 restored to the twilight zone and the vertical NO_3 flux into the euphotic zone. The κ_{di} profile (black line) is highest above z_{eu} and attenuates rapidly with depth. The purple shading in Figures 5a to 5c represent the concentration of NO_3 with depth, and the slope (S_N) of these contours relative to the horizontal is shown in Figure 5b. The tilted black lines represent the fixed isopycnal angle (S_σ). The normalized relative difference between S_σ and S_N varies from 1 (Figure 5a) to 0 (Figure 5c). Depending on the choice of κ_{iso} and κ_{di} (the two free parameters), the NO_3 alignment with σ_t lies somewhere between these two extremes (Figure 5b).

occurs along isopycnal surfaces in the pycnocline and tends to homogenize (decrease gradients in) NO_3 on isopycnal surfaces even where density surfaces are tilted. The intensity of eddy-driven fluxes varies in space and time, and is often parameterized by an isopycnal eddy diffusivity, κ_{iso} [*Ledwell et al.*, 1993, 1998; *Abernathey and Marshall*, 2013]. Where the eddy-diffusivity is large, the along-isopycnal homogenization by advective processes leads to the realignment of nitrate along density surfaces. Where the biological pump is strong, and the depth-dependent redistribution of nitrate occurs more rapidly than the along-isopycnal homogenization by eddies, we expect the nitrate to deviate from isopycnal alignment.

4.1. Model for Alignment of Nitrate with Isobars or Isopycnals

[24] We propose a model to explore qualitatively the competition between sinking and remineralization of particulate organic matter that distributes nitrate in a depth-dependent fashion on isobars, and along-isopycnal mixing that aligns nitrate with isopycnals (Figure 5).

[25] The model domain spans from the surface to −800 m and 40 km horizontally, with the top of the twilight zone (the base of the euphotic depth) at −80 m. Isopycnals are tilted with a fixed slope of $S_\sigma = 1.6 \times 10^{-3}$, corresponding to a vertical excursion of 160 m over 100 km. This excursion is typical of the large-scale variations in isopycnal depth observed from the WOA09 data at high latitudes (see Figure 2a). NO_3 is initially oriented along isopycnals, linearly increasing from 2 μM at the shallowest isopycnal to 50 μM at −800 m. The model is periodic at the sides, no flux of NO_3 is permitted through the surface ($z = 0$), and the concentration at −800 m is kept fixed at 50 μM. The modeled NO_3 is evolved from the initial conditions according to

$$\frac{\partial NO_3}{\partial t} = \underset{(a)}{\nabla(\kappa \nabla NO_3)|_{\sigma_t = const}} - \underset{(b)}{\frac{F_z}{z_{eu}}|_{z<z_{eu}}} + \underset{(c)}{r\, exp\left(\frac{-z}{L}\right) NO_3}. \quad (3)$$

[26] The model equation is discretized using finite volumes and solved numerically. The terms on the right hand side represent (a) redistribution due to along isopycnal and diapycnal mixing, (b) consumption of NO_3 that is vertically fluxed (F_z) into the euphotic zone, and (c) restoration of NO_3 due to particle export and remineralization. At each time step, NO_3 is converted from the z-coordinate system to an isopycnal coordinate system, and (a) is computed by mixing NO_3 along (κ_{iso}) and across (κ_{di}) isopycnals. The NO_3 consumption scales with the vertical flux at the base of the euphotic zone (F_z), which is the sum of the vertical contributions to flux from the along and diapycnal eddy diffusivity. We find that for the small isopycnal slope ($S_\sigma = 1.6 \times 10^{-3}$) used here, the vertical component of the along-isopycnal flux is negligible compared to the vertical component of the diapycnal flux. We estimate F_z according to

$$F_z \simeq \kappa_{di} \frac{\partial NO_3}{\partial z}, \quad (4)$$

taking the first difference between NO_3 at -60 and -100 m (spanning the euphotic base). We prescribe a diapycnal diffusivity that is largest within the euphotic zone and decreases with an e-folding scale of 20 m (see κ_{di} profile in Figure 5). The along-isopycnal eddy diffusivity is constant everywhere. Nitrate is resupplied in an exponentially decaying fashion, with a fixed remineralization depth (L) of 200 m similar to the value estimated from observations [*Lutz et al.*, 2002] and used in models [*Kwon et al.*, 2009]. The restoration rate (r) at $z = z_{eu}$ is set so that the total NO_3 that is resupplied, matches the total NO_3 removed at each time step. Thus we balance removal by the upward flux into the euphotic zone with resupply through export and remineralization.

[27] The model has two free parameters; κ_{iso} which tends to homogenize NO_3 on isopycnals, and κ_{di} which controls the vertical flux of NO_3 past z_{eu}, and thereby the export and resupply of NO_3 with depth. We explore seven values for the near-surface κ_{di} (0.0009, 0.0014, 0.0023, 0.0035, 0.0046, 0.0070, and 0.0116 $m^2 s^{-1}$) and 10 values for κ_{iso}, logarithmically distributed between 10^2 and 10^4 $m^2 s^{-1}$, a range that is consistent with published horizontal diffusivities [*Abernathey and Marshall*, 2013]. The model is time integrated with a time step of 0.25 d until it reaches steady state, where the rate of change of NO_3 at each grid point is $<10^{-9}$ $\mu M s^{-1}$ (which occurs over model weeks to one year).

[28] We find that at steady-state, NO_3 iso-surfaces become oriented horizontally when κ_{iso} is weak relative to κ_{di} (i.e., Figure 5a), and oriented parallel to isopycnals when κ_{iso} is strong (i.e., Figure 5c). In this model, the NO_3 slope is such that $0 \leq S_N \leq S_\sigma$ (i.e., Figure 5b). We average S_N and S_σ across the model domain between $z = -150$ and -250 m, and find the normalized difference according to

$$R = \frac{\overline{S_\sigma} - \overline{S_N}}{\overline{S_\sigma}}. \quad (5)$$

[29] R for three different κ_{di} cases is shown as a function of κ_{iso} (Figure 6a). For weak $\kappa_{iso} = 100$ $m^2 s^{-1}$, and strong $\kappa_{di} = 0.0046$ $m^2 s^{-1}$ R $\sim$1 (red line, Figure 6a), indicating that the NO_3 iso-surfaces are nearly horizontal. As κ_{iso} is increased, R approaches zero, as the NO_3 iso-surfaces became parallel with the isopycnals. The nitrogen export out of the euphotic zone is constrained so that it balances the vertical supply of NO_3. We can produce a carbon-based estimate of the particle export $= 12\frac{106}{16} F_z$ for each model run. The transition where $R = 0.5$ (horizontal dashed line and colored circles, Figure 6a), indicates the threshold where isopycnal mixing and the export are balanced such that the NO_3 iso-surfaces lie halfway between the horizontal and the fixed isopycnals. The particle export computed from each κ_{di} at this transition is indicated by the corresponding colored points in Figure 6b.

[30] The physical interpretation of the model transition ($R = 0.5$, and the diagonal fit in Figure 6b) is that for the given isopycnal slope and remineralization depth, scenarios of κ_{iso} and export that fall above this line will have greater NO_3 alignment with the horizontal, and cases that fall below this line with have greater NO_3 alignment with isopycnals. We qualitatively compare this modeled threshold with the range of observed estimates of κ_{iso} and particle export (dashed oval region, Figure 6b). Overall, we find that the particle export required to counteract eddy diffusivity is much larger than what is typically observed in the ocean (i.e., the dashed region in Figure 6b falls well below the transition line predicted by the model). Although the model is highly idealized and does not encompass the full range of biological and physical scenarios, it suggests that with the observed oceanic ranges of export and κ_{iso}, along-isopycnal mixing dominates the orientation of isonitrate surfaces.

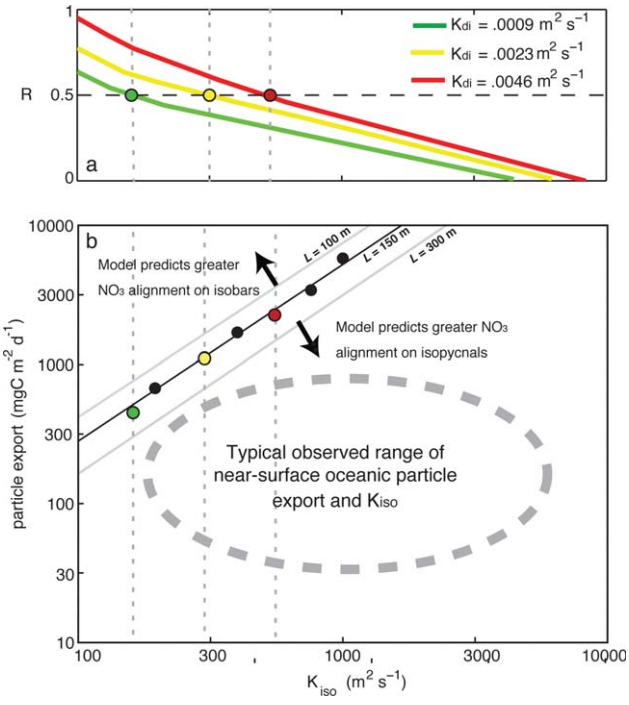

Figure 6. Steady state model-derived (a) $R = \frac{S_\sigma - S_N}{S_\sigma}$ versus κ_{iso}. Three cases with different κ_{di} are shown in colored lines. The inferred carbon export for each case is 451 (green), 1127 (yellow), and 2263 (red) mgC $m^{-2} d^{-1}$, respectively. The intersection these curves with $R = 0.5$ (colored points), indicates the transition from alignment on isobars to isopycnals as the isopycnal mixing (κ_{iso}) is increased. (b) The modeled export required to balance the modeled κ_{iso} and maintain the NO_3 isolines at the transition $R = 0.5$ (colored and black points). These follow a power-law fit, with $L = 150$ m (solid black line). Corresponding fits with $L = 100$ and 300 m are shown (grey lines). The dashed gray circle represents the general range of export and κ_{iso} that are observed across a variety of oceanic regimes.

4.1.1. Sensitivity to the Isopycnal Slope and the Remineralization Depth

[31] We tested the sensitivity of the model results to the initial NO_3 conditions, the fixed isopycnal slope (S_σ), and the remineralization depth (L). The results are insensitive to the initial NO_3 gradient and orientation. We vary S_σ between 0.001 and 0.01. For isopycnal slopes of 0.005, the transition line (from Figure 6b) is shifted upward, requiring

roughly a 50% larger particle export. At smaller angles, the transition line is lowered. The minimum S_σ we can resolve in our model setup is 0.001, and for this isopycnal angle, the transition line is lowered by roughly 15%, remaining above the typical observed oceanic export and κ_{iso} ranges (dashed circle, Figure 6b).

[32] The e-folding remineralization depth (L), may be influenced by a range of biological and environmental factors, including temperature, nutrient availability, particle size, the phytoplankton and consumer communities, and their vertical distributions [*Micheals and Silver*, 1988]. *Laws et al*. [2000] suggests that temperature may be the primary determinant of how much of the primary production goes into export production (as reflected by sea surface temperature [SST] dependance in the *pe*-ratio in equation (9) below). Metabolic rates increase with temperature, thus tending to reduce the growth efficiency for marine bacteria [*Rivkin and Legendre*, 2001] and zooplankton [*Ikeda*, 1985]. Organic particulates are more slowly degraded at lower temperatures, thus allowing a more efficient export and a deeper remineralization depth. Here, we model export according to an exponential profile with a remineralization depth (L) of 150 m. This length scale is directly related to the export efficiency, the ratio between the particulate organic carbon (POC) flux 100 m below z_{eu} and the surface net primary production (NPP) [*Buessler and Boyd*, 2009]. Observations over a broad range of export regimes indicate that this ratio varies between 0.05 and 0.40, corresponding to a range in possible L from $z_{eu} + 105$ to $z_{eu} + 150$ m. Thus, we explore the sensitivity of our model to a range in L from 100 to 300 m. At $L = 100$ m the transition line is shifted up, requiring a larger export to transition NO_3 onto isobars. At $L = 300$ m the transition line is shifted down, closer to the typical ranges of oceanic export and κ_{iso} (solid gray lines, Figure 6b). Overall, we find that the model results depend on both isopycnal slope (S_σ) and remineralization depth (L). We explore the results over the range of S_σ and L likely to occur in the ocean, and find that for most cases, isopycnal mixing is still expected to dominate the isonitrate orientation.

5. Explaining the Orientation of Nitrate Surfaces in the Global Data

[33] The model described in the previous section assumes no horizontal variation in κ_{iso}, or the biological pump, and therefore, S_N always lies between 0 and S_σ. In the ocean, the strength of the biological pump varies horizontally, and lateral sources of NO_3 exist (e.g., from riverine runoff), enabling nitrate-surfaces to become steeper than the isopycnals. Therefore, ΔS is defined as the absolute value of the difference $\Delta S = |S_\sigma - S_N|$ (Figure 7a). We find that ΔS is minimum (less than 10^{-5} and indistinguishable from zero) in the midlatitudes. Conversely, ΔS is elevated in the productive regions of the North Atlantic, throughout the equatorial upwelling regions, and in the iron-limited Southern Ocean. Our hypothesis is that large departures in isonitrate surfaces from isopycnals in the twilight zone (here, centered at 560 m depth) represent locations where the biological pump is strong, and imposes a depth-dependent distribution of NO_3. A relative increase in the redistribution of nitrate by along-isopycnal mixing compared to the biological pump, reorients nitrate along density surfaces. To test this hypothesis in the global setting, we obtain estimates of the global eddy diffusivity (κ_{iso}) and export flux, to assess the strength of competing processes that control NO_3 in the twilight zone.

5.1. Estimate of Global Eddy Diffusivities κ_{iso}

[34] A number of studies have developed methods for estimating κ_{iso} globally [*Holloway*, 1986; *Zhurbas and Oh*, 2004; *Abernathey and Marshall*, 2013], with recent studies focusing on suppression of diffusivity in jets in the Antarctic circumpolar current (ACC) region [*Naveira Garabato et al*., 2011; *Karsten and Marshall*, 2002; *Klocker et al*., 2012].

[35] Here, we use a zeroth-order method, that aims to capture the large scale variability and order of magnitude of κ_{iso} globally. We follow the scaling suggested in *Holloway* [1986] and *Karsten and Marshall* [2002]. In this case, κ_{iso} is assumed to be proportional to the root mean square of the geostrophic stream function variability (ψ'). This variability is parameterized though the corresponding sea surface height variance (h'^2) such that

$$\kappa_{iso} = \gamma\sqrt{\overline{\psi'^2}} = \gamma\frac{g}{f}\sqrt{\overline{h'^2}}, \tag{6}$$

where g is the acceleration due to gravity, f is the coriolis frequency and γ is a constant of proportionality. Following *Karsten and Marshall* [2002], we use $\gamma = 0.26$. We obtain global AVISO (http://www.aviso.oceanobs.com) h'^2 from the weekly data spanning from March 1995 to December 2004, and compute κ_{iso} (Figure 7b). At low latitudes, f approaches zero and κ_{iso} from becomes unrealistically large (equation (6)). Thus, within 20° latitude, we keep f constant at $f(\text{lat} = 20^\circ) = 4.99 \times 10^{-5}$ s^{-1}, which gives κ_{iso} values comparable to modeled estimates of roughly 2000 to 6000 m^{2}s^{-1} [*Abernathey and Marshall*, 2013] within this band. The κ_{iso} estimates are then binned onto the $5^\circ \times 5^\circ$ WOA09 grid (Figure 7b).

[36] The isopycnal diffusivity κ_{iso} may be suppressed in regions of strong currents and may vary with depth [*Klocker et al*., 2012]. However, in the ACC, κ_{iso} at 600 m depth (the twilight zone depth that we explore here) tends to be within 20% of the surface value [*Klocker et al*., 2012]. This variation in the vertical is small compared with the large-scale spatial variability and is neglected by us, since we use surface data. The spatial patterns and magnitudes of κ_{iso} that we obtain and use, i.e., $\sim$400$-$1000 m^{2}s^{-1} in the ACC [*Klocker et al*., 2012], 1500 to 4000 m^{2}s^{-1} in the North Pacific [*Holloway*, 1986], are similar in magnitude to other published estimates and very similar in spatial pattern to the modeled eddy diffusivities of *Abernathey and Marshall* [2013].

5.2. Estimate of the Global POC Export

[37] NPP is the sum of the production due to recycled sources of nitrogen within the euphotic zone, and that fueled by the supply of fresh nitrate (new production). A large fraction of the new production is associated with NO_3 that is fluxed vertically from the twilight zone into the euphotic zone. We hypothesize that deviations between the isosurfaces of NO_3 and σ_t may be enhanced in locations

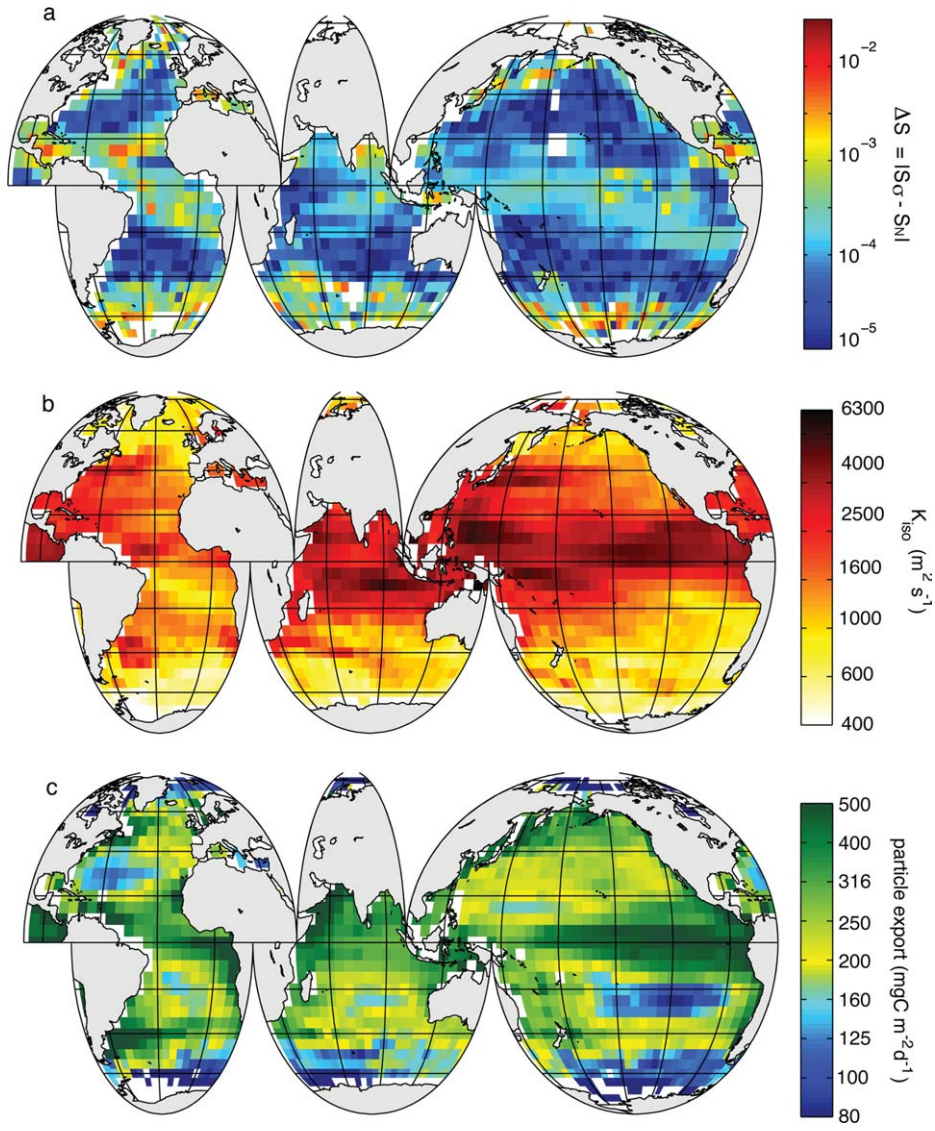

Figure 7. Maps of (a) the isopycnal-nitrate slope deviation (ΔS), (b) κ_{iso} ($m^2 s^{-1}$) following *Karsten and Marshall* [2002], and (c) Annually averaged particle export (mgC $m^{-2}d^{-1}$) estimated from Seawifs CbPM2 and the *pe*-ratio model of *Dunne et al*. [2005]. Both κ_{iso} and export are binned onto the $5^\circ \times 5^\circ$ WOA09 grid.

where the POC export is large, and the remineralization processes redistribute NO_3 in the twilight zone, independent of the isopycnal slope. We assume that remineralization of nitrogen and carbon vary according to a Redfield ratio [*Anderson and Sarmiento*, 1994], and evaluate spatial variations of the annually averaged export (and NPP) in units of mgC $m^{-2}d^{-1}$. We obtain an estimate of the POC export from a carbon-based productivity (NPP) model (CbPM2, *Westberry et al*. [2008]), and a *pe*-ratio model. The ratio between the particle export and the NPP is termed the *pe*-ratio according to

$$\text{Particle Export} = \text{NPP} \times \textit{pe}\text{-ratio}. \quad (7)$$

[38] The CbPM2 model for NPP is developed from Level 3, 8-day binned SeaWiFS products; Garver-Siegel-Maritorena chlorophyll and particle backscatter [*Maritorena et al*., 2002], light attenuatzion depth (K_{490}) and photosynthetically available radiation. The CbPM2 products are available at ftp://ftp.oceancolor.ucsb.edu//pub/org/oceancolor/MEaSUREs/NPP/Monthly/CBPM2/Seawifs/.

[39] To obtain a global estimate of the *pe*-ratio, we use Level 3, 9 km, monthly SST, the K_{490} climatology from MODIS (data available at http://oceancolor.gsfc.nasa.gov), and NPP from the CbPM2 product. We use the empirical *pe*-ratio model of *Dunne et al*. [2005],

$$\textit{pe}\text{-ratio} = -0.0101\, SST + 0.0582 \log\left(\frac{NPP}{Z_{eu}}\right) + 0.419 \quad (8)$$

for $0.04 < \textit{pe}\text{-ratio} < 0.72$. The monthly climatological *pe*-ratio is then averaged into an annual mean, and binned onto the $5 \times 5^\circ$ WOA09 grid. The product of the NPP and *pe*-ratio provides an estimate of the mean global POC

export flux (Figure 7c). We find that the POC export flux typically varies between 100 and 1000 mgC $m^{-2}d^{-1}$ with elevated values in equatorial regions, coastal upwelling systems and western boundaries. The range and spatial patterns are consistent with previously modeled POC export estimates [e.g., *Moore et al.*, 2004].

5.3. Slope of Isonitrate Surfaces

[40] While biological production and sinking and remineralization of organic matter tends to distribute nitrate in a depth-dependent manner, we expect isopycnal mixing to align nitrate with density surfaces. To test this with oceanic data, we examine the density-nitrate slope deviations ΔS against the eddy diffusivity and particle export estimated from satellite data (Figure 7).

[41] The ranges of κ_{iso} and particle export are each divided into 40 logarithmically spaced bins, and the median ΔS within each bin is shown within this parameter space (Figure 8). Recall that the median ΔS is roughly $10^{-3.5}$. We find that ΔS varies based on both κ_{iso} and export. In regions where the particle export is larger than 300 mgC $m^{-2}d^{-1}$, ΔS is anomalously high, ranging between $10^{-3.5}$ and 10^{-2}. Similarly, where κ_{iso} is less than 1000 m^2s^{-1}, ΔS is also elevated. Where κ_{iso} is greater than 1000 m^2s^{-1} and the particle export is less than 300 mgC $m^{-2}d^{-1}$, ΔS is low, suggesting a high degree of alignment of NO_3 with isopycnals.

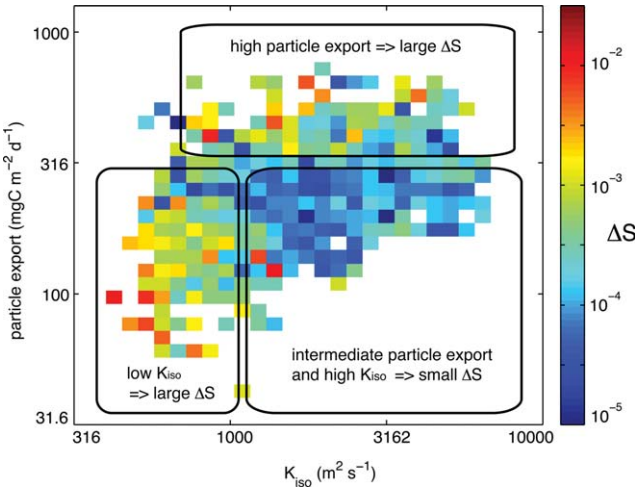

Figure 8. Binned particle export versus κ_{iso} seen in Figures 4b and 4c. Colors indicate the median ΔS in each bin (see Figure 4a). The ΔS data falls into three regions; elevated ΔS in locations of either high particle export, or low κ_{iso}. Conversely, ΔS is low where the particle export is intermediate and κ_{iso} is relatively large. Log-transformed κ_{iso} and particle export are significantly positively correlated with $r^2 = 0.25, p < 0.001$.

6. Summary and Discussion

[42] Oceanic nitrate is known to correlate more strongly with density than with depth, though the biological pump tends to redistribute nitrate in a depth dependent fashion. Reduced variance of nitrate on isopycnals, as compared to isobars, is often ascribed to the vertical movement of isopycnal surfaces [*While and Haines*, 2010; *Ascani et al.*, 2013]. We show in fact, a significant alignment between isonitrate and isopycnal surfaces persists in time-averaged data at large scales. We hypothesize that it is the along-isopycnal eddy fluxes that generate this alignment in spite of the nitrate sources and sinks being depth dependent and locally horizontally varying. The slope of the isonitrate surfaces relative to isopycnals can vary regionally, and the relative magnitude of the variance on isopycnals and isobars can also vary vastly from one region to another. Using a simple model, we show that the relative strength of the along-isopycnal diffusive flux compared to the depth-dependent (biological) redistribution determines the slope of the isonitrate surfaces. Large along-isopycnal eddy diffusivity leads to better alignment of isonitrate surfaces with isopycnals, while a stronger biological pump (which results from higher diapycnal fluxes) results in flatter isonitrate surfaces. Using satellite data to estimate the export production and horizontal (along-isopycnal) diffusivity, we find that the relative strengths of the diagnosed processes substantiate our hypothesis.

[43] In our model, we neglect horizontal variability in the vertical sources and sinks for nitrate. Hence, the nitrate surfaces vary from being flat to being perfectly aligned with isopycnals. In the ocean, horizontal variability in the biological processes, or sources for nitrate (for example, terrestrial runoff) can generate horizontal gradients that tend to steepen nitrate surfaces. In certain regions, this may counter the tendency to flatten isopycnals, or could make the nitrate surfaces even steeper than isopycnals. Metabolic rates are controlled by temperature, thus impacting the export efficiency. We explored model scenarios that covered a range in remineralization depths expected due to the global range in SST and observed export efficiencies. However, the export of sinking particles is likely affected by different stratification conditions due to a vertical gradient in remineralization rates, or by suspension of particulates at neutral density. These possibilities were not addressed in the idealized model presented here. The impact of stratification on the fate of sinking particles is not well known, and may also play a role in the large scale alignment of nitrate through remineralization of density-neutral particles or dissolved organic matter.

[44] Our estimate of export production from satellite data only takes into account vertical export. Lateral sources/sinks for nitrate are excluded from this satellite-based estimate, which is used to compare the processes that cause deviation of the nitrate surfaces from isopycnals. The temporal variability in the satellite data is also neglected. We compare the strength of this vertical, depth-dependent flux with κ_{iso}. A more appropriate comparison would be with the diffusive flux, but its computation would also need to include the horizontal (along-isopycnal) gradient of nitrate. The annual mean nitrate distribution is used to estimate the isonitrate surface slope, since the seasonal variability is negligible at depth.

[45] The magnitudes of the depth-dependent sources/sinks of nitrate in our model are not explicitly specified, but related to the strength of the diapcynal diffusivity. In the ocean too, when nitrate is a limiting nutrient, the strength of the vertical transport determines the uptake rate of nitrate, and consequently the export flux. Thus, in a gross

sense, it is the ratio of the isopycnal diffusivity to diapcynal diffusivity that determines the alignment of isonitrate surfaces with isopycnals.

[46] Large-scale ocean models often initialize or restore nitrate on isobars or isopycnals. Here, we show that the orientation of nitrate surfaces relative to the horizontal and the isopycnals may vary regionally. But in most regions, horizontal (eddy) diffusive fluxes dominate over the depth-dependent sources and sinks, and at large scales, nitrate is persistently more aligned with isopycnals than isobars.

[47] **Acknowledgments.** We acknowledge the support of the National Science Foundation (Grant OCE-0928617) and NASA (Grant NNX-08AL80G) and feedback from K. H. Brink and two peer-reviewers.

References

Abernathey, R. P., and J. Marshall (2013), Global surface eddy diffusivities derived from satellite altimetry, *J. Geophys. Res.*, *118*, 1–16.

Anderson, L. A., and J. L. Sarmiento (1994), Redfield ratios of remineralization determined by nutrient data analysis, *Global Biogeochem. Cycles*, *8*(1), 65–80.

Ascani, F., K. J. Richards, E. Firing, S. Grant, K. S. Johnson, Y. Jia, R. Lukas, and D. M. Karl (2013), Physical and biological controls of nitrate concentrations in the upper subtropical North Pacific Ocean, *Deep Sea Res. Part II*, *93*, 119–134.

Bretherton, F. P., R. E. Davis, and C. B. Fandry (1976), A technique for objective analysis and design of oceanographic experiments applied to MODE-73, *Deep Sea Res.*, *23*, 559–582.

Buessler, K. O., and P. W. Boyd (2009), Shedding light on processes that control particle export and flux attenuation in the twilight zone of the open ocean., *Limnol. Oceanogr.*, *54*(4), 1210–1232.

de Boyer Montégut, C., G. Madec, A. Fischer, A. Lazar, and D. Iudicone (2004), Mixed layer depth over the global ocean: An examination of profile data and a profile-based climatology, *J. Geophys. Res.*, *109*, C12003, doi:10.1029/2004JC002378.

Dunne, J. P., R. A. Armstrong, A. Gnanadesikan, and J. L. Sarmiento (2005), Empirical and mechanistic models for the particle export ratio, *Global Biogeochem. Cycles*, *19*, GB4026, doi:10.1029/2004GB002390.

Garcia, H. E., R. A. Locarnini, T. P. Boyer, J. I. Antonov, M. M. Zweng, O. K. Baranova, and D. R. Johnson (2010), *World Ocean Atlas 2009, Volume 4: Nutrients (phosphate, nitrate, silicate)*, edited by S. Levitus, NOAA Atlas NESDIS 71, U.S. Government Printing Office, Silver Spring, Md.

Goes, J. I., T. Saino, H. Oaku, J. Ishizaka, C. S. Wong, and Y. Nojiri (2000), Basin scale estimates of sea surface nitrate and new production from remotely sensed sea surface temperature and chlorophyll, *Geophys. Res. Lett.*, *27*(9), 1263–1266.

Holloway, G. (1986), Estimates of oceanic eddy transports from satellite altimetery, *Nature*, *323*(18), 243–244.

Ikeda, T. (1985), Metabolic rates of epipelagic marine zooplankton as a function of body mass and temperature, *Mar. Biol.*, *85*(1), 1–11.

Johnson, K. S., S. C. Riser, and D. M. Karl (2010), Nitrate supply from deep to near-surface waters of the North Pacific subtropical gyre, *Nature*, *465*(7301), 1062–1065.

Johnson, K. S., L. J. Coletti, H. W. Jannasch, C. M. Sakamoto, D. D. Swift, and S. C. Riser (2013), Long-term nitrate measurements in the ocean using the In Situ Ultraviolet Spectrophotometer: sensor integration into the Apex profiling float, *J. Atmos. Oceanic Technol.*, *30*, 1854–1866.

Kamykowski, D., and S. J. Zentara (1985), Nitrate and silicic acid in the world ocean: Patterns and processes, *Mar. Ecol. Prog. Ser.*, *26*, 47–59.

Karsten, R. H., and J. Marshall (2002), Constructing the residual circulation of the ACC from observations, *J. Phys. Oceanogr.*, *32*, 3315–3327.

Klocker, A., R. Ferrari, and J. H. LaCasce (2012), Estimating suppression of eddy mixing by mean flows, *J. Phys. Oceanogr.*, *42*(9), 1566–1576.

Kwon, E. Y., F. Primeau, and J. L. Sarmiento (2009), The impact of remineralization depth on the air–sea carbon balance, *Nature Geosci.*, *2*(9), 630–635.

Laws, E. A., P. G. Falkowski, W. O. Smith, Jr, H. Ducklow, and J. J. McCarthy (2000), Temperature effects on export production in the open ocean, *Global Biogeochem. Cycles*, *14*, 1231–1246.

Ledwell, J. R., A. J. Watson, and C. S. Law (1993), Evidence for slow mixing across the pycnocline from an open-ocean tracer-release experiment, *Nature*, *364*, 1–3.

Ledwell, J. R., A. J. Watson, and C. S. Law (1998), Mixing of a tracer in the pycnocline, *J. Geophys. Res.*, *103*(C10), 21,499–21,529.

Levitus, S., M. E. Conkright, J. L. Reid, R. G. Najjar, and A. Mantyla (1993), Distribution of nitrate, phosphate and silicate in the world oceans, *Prog. Oceanogr.*, *31*, 245–273.

Lucas, A. J., C. L. Dupont, V. Tai, J. L. Largier, B. Palenik, and P. J. S. Franks (2011), The green ribbon: Multiscale physical control of phytoplankton productivity and community structure over a narrow continental shelf, *Limnol. Oceanogr.*, *56*(2), 611–626.

Lutz, M., R. Dunbar, and K. Caldiera (2002), Regional variability in the vertical flux of particulate organic carbon in the ocean interior, *Global Biogeochem. Cycles*, *16*(3), doi:10.1029/2000GB001383.

Maritorena, S., D. A. Siegel, and A. R. Peterson (2002), Optimization of a semianalytical ocean color model for global-scale applications, *Appl. Opt.*, *41*(15), 2705–2714.

Micheals, A. F., and M. W. Silver (1988), Primary production, sinking fluxes and the microbial food web, *Deep Sea Res.*, *35*(4), 473–490.

Moore, J. K., S. C. Doney, and K. Lindsay (2004), Upper ocean ecosystem dynamics and iron cycling in a global three-dimensional model, *Global Biogeochem. Cycles*, *18*, GB4028, doi:10.1029/2004GB002220.

Naveira Garabato, A. C., R. Ferrari, and K. L. Polzin (2011), Eddy stirring in the Southern Ocean, *J. Geophys. Res.*, *116*, C09019, doi:10.1029/2010JC006818.

Rivkin, R. B., and L. Legendre (2001), Biogenic carbon cycling in the upper ocean: Effects of microbial respiration, *Science*, *291*(5512), 2398–2400.

Switzer, A. C., D. Kamykowski, and S.-J. Zentara (2003), Mapping nitrate in the global ocean using remotely sensed sea surface temperature, *J. Geophys. Res.*, *108*(C8), 3280, doi:10.1029/2000JC000444.

Westberry, T., M. J. Behrenfeld, D. A. Siegel, and E. Boss (2008), Carbon-based primary productivity modeling with vertically resolved photoacclimation, *Global Biogeochem. Cycles*, *22*, GB2024, doi:10.1029/2007GB003078.

While, J., and K. Haines (2010), A comparison of the variability of biological nutrients against depth and potential density, *Biogeosciences*, *7*, 1263–1269.

Zhurbas, V., and I. S. Oh (2004), Drifter-derived maps of lateral diffusivity in the Pacific and Atlantic Oceans in relation to surface circulation patterns, *J. Geophys. Res.*, *109*, C05015, doi:10.1029/2003JC002241.